Supplementary Information for Coupling among Growth Rate Response, Metabolic Cycle and Cell Division Cycle in Yeast

Nikolai Slavov[1,§], and David Botstein[1,§]
1 Princeton University, Princeton, NJ 08544, USA
[§]Corresponding authors: nslavov@alum.mit.edu, botstein@princeton.edu

1 Controlling the Growth Rate in Chemostats

A population of microorganisms growing in the wild (or in a test tube) is likely to be composed of cells growing at different growth rates and changing their growth rate in time as nutrients are being depleted or other physical parameters (such as temperature) change in time. Studying the physiological responses to changes in growth rate is thus greatly confounded by many factors that might be unobserved and changing in time. The chemostat (Novick and Szilard, 1950) is a convenient experimental apparatus allowing one to avoid such complications. In its essential design, a chemostat is a fermenter for continuous cultures with a constant influx of fresh nutrient media and equal efflux of reaction media containing cells, residual nutrients and secreted metabolites, Fig.S1.

The dynamics of a chemostat cultures can be modeled by a very simple ordinary differential equation (1) with a single dependent variable N denoting the number of cells and the time t being the independent variable.

$$\frac{dN}{dt} = \mu N - DN \tag{1}$$

Equation (1) describes the change in the number of cells N as a function of the growth rate of the population μ and the dilution data D. At steady–state $dN/dt = 0$ and thus the growth rate equals the dilution rate, $\mu = D$. This is an important result and equation (1) is the simplest way to derive it. However, equation (1) is rather limited in describing dynamics because the growth rate itself is a function of the growth conditions and the nutrient concentrations which are not included in equation (1). Equation (1) cannot even predict how the steady–state biomass density depends on the concentration of nutrients in the media.

These limitation can be overcome by only slightly more complicated model with two first–order ordinary differential equations (2–3) assuming that the growth rate dependence on the nutrient concentration can be described

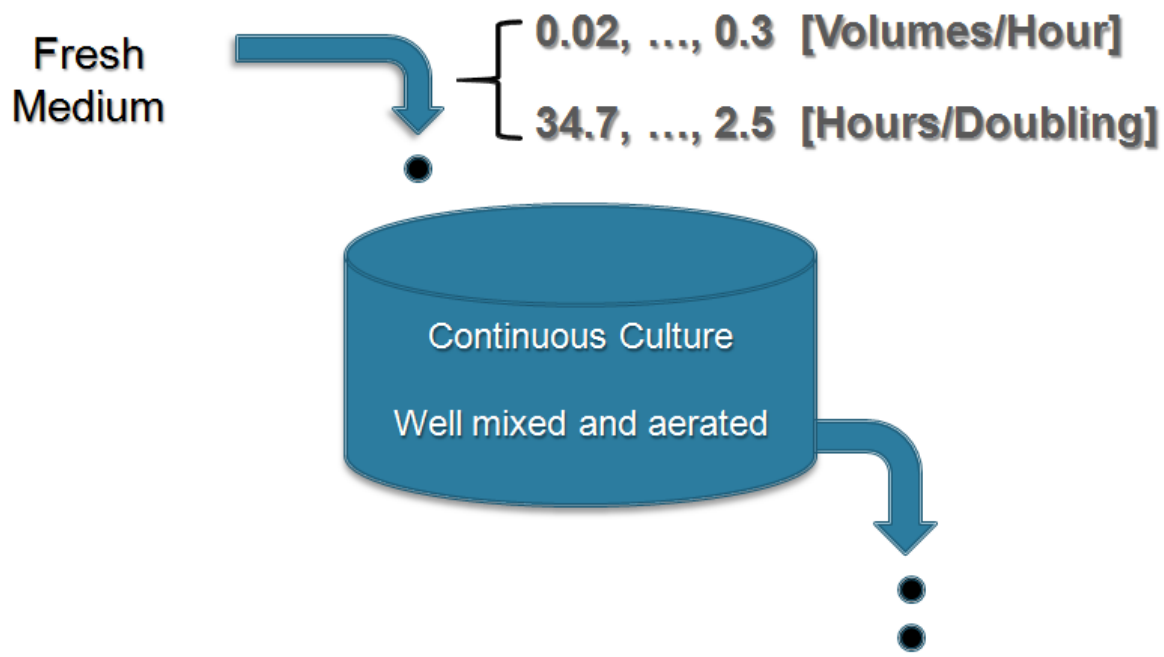

Figure 1. Schematic diagram of a chemostat (Novick and Szilard, 1950).

by a Monod equation (Monod, 1942, 1949).

$$\frac{dS}{dt} = D(S_o - S) - \frac{1}{\gamma} N \mu_{max} \frac{S}{S+K} \tag{2}$$

$$\frac{dN}{dt} = N \mu_{max} \frac{S}{S+K} - DN \tag{3}$$

The 2 dependent variables are the number of cells (N) and the amount of nutrient substrate (S) in the fermenter vessel. For simplicity and enhanced experimental control, it is convenient to provide all nutrients except for one in excess so that the growth of the culture depends only on the nutrient that is limited. Thus in Eq. (2–3), S is the amount of limiting nutrient. It is often more convenient to work with the concentration of the limiting nutrient and the biomass density (number of cells or cell volume per unit volume) rather than the absolute amounts. Making this change in Eq. (2–3) requires a simple scaler scaling by the volume and changes only the unites of N and S.

In the model above Eq. (2–3), the dynamics of N and S depend on four parameters:

- S_o – concentration of the limiting nutrient in the feed (fresh media)
- μ_{max} – The highest growth rate that the organisms can archive if all nutrients are abundant, e.g. above saturating nutrient concentrations.
- γ – A parameter quantifying the efficiency of converting the limiting nutrient into biomass. For example, grams of biomass generated from a gram of glucose.
- D – Dilution rate. The rate at which new media drips into the chemostat. By design, D is also the rate at

which reaction media leaves the fermenter vessel.

At steady–state $dN/dt = 0$. Setting the derivative equal to zero in Eq. (3), results in:

$$\mu = \mu_{max} \frac{S}{S + K} = D \tag{4}$$

Thus, at steady–state the growth rate of the chemostat culture (μ) equals the dilution rate. Since the dilution rate can be set conveniently by the experimenter, this allows growing a culture at any desired growth rate that does not exceed μ_{max}. Solving equations (2–3) for steady–state enables expressing the steady–state biomass as a function of the concentration of the limiting nutrient in the media which will be used in the following sections.

2 Experimental Design

One of the crucial factors in measuring the growth rate response accurately is using yeast strains and growth conditions that allow for a wide dynamical range of growth rates. Very slow growth rates are harder to establish and maintain accurately in a chemostat because small leaks of the pumps or obstructions of the tubing become significant relative to the set dilution rate. Furthermore, the physiological state of the cells approaches asymptotically *G1/G0* arrest (quiescence) and measured changes become comparable to inevitable fluctuations associated with experimental measurements. As a result, at very slow growth rate the signal to noise ratio *(SNR)* decreases to rather unfavorable level. Thus to generate high quality data, it is highly desirable to extend the dynamical range of the growth rates by using strains and conditions allowing short doubling times. Initially, we started the experiments with *WT CEN.PK*. Its maximal growth rate on ethanol is rather slow and this not only fundamentally limited the dynamical range of our experiments but also resulted in rather low biomass densities even at $\mu = 0.08h^{-1}$. To overcome this problem, we looked for a strain that can grow faster on ethanol. Such a strain was isolated by Thomas Fox for its ability to grow well on ethanol (Fig.S2) and cataloged as *DBY11369* in the strain collection of David Botstein. We used *DBY11369* for all growth rate experiments on ethanol carbon source described in the paper. In excess of all nutrients (exponential phase in a batch culture) and at 30^oC, the highest growth rate we measured with *DBY11369* is $\mu = 0.15h^{-1}$ (Fig.S2) which is higher than the growth rate we measured with any of the other strains we grew including *WT CEN.PK* and *WT S288C, HAP1*$^+$.

A second important consideration in our experimental design was finding nutrient concentrations that are both limiting and result in optimal biomass densities at steady–state. As already mentioned, limiting the growth of the culture on a single nutrient simplifies the control of the experiment and the analysis of the data. In particular, solving Eq. (2–3) at steady–state ($dS/dt = dN/dt = 0$), indicates that the steady–state biomass depends linearly on S_0, the concentration of the limiting nutrient in the fresh media. To establish optimal concentrations for limiting nutrients, we grew *DBY11369* in batch in chemostat media with varying amounts of the limiting nutrient. Fig.S3 shows the final biomass (the biomass of the culture after the growth stops and the biomass density reaches an asymptotic value) as a function of the ethanol concentration: To quantify the biomass, we used OD_{600}, the absorbance (optical density) of the culture for light with wavelength $\lambda = 600nm$. Since we scanned a wide dynamical range of limiting nutrient concentrations, the biomass also varied widely, reaching high levels at which the optical density is not linearly proportional to the biomass density. To avoid such aberrations, we did serial dilutions ensuring that for all datapoints the measured optical density is close to the optimum of the spectrophotometer. Fig.S3 shows that the final biomass depends linearly on the concentration of ethanol over a wide dynamical range.

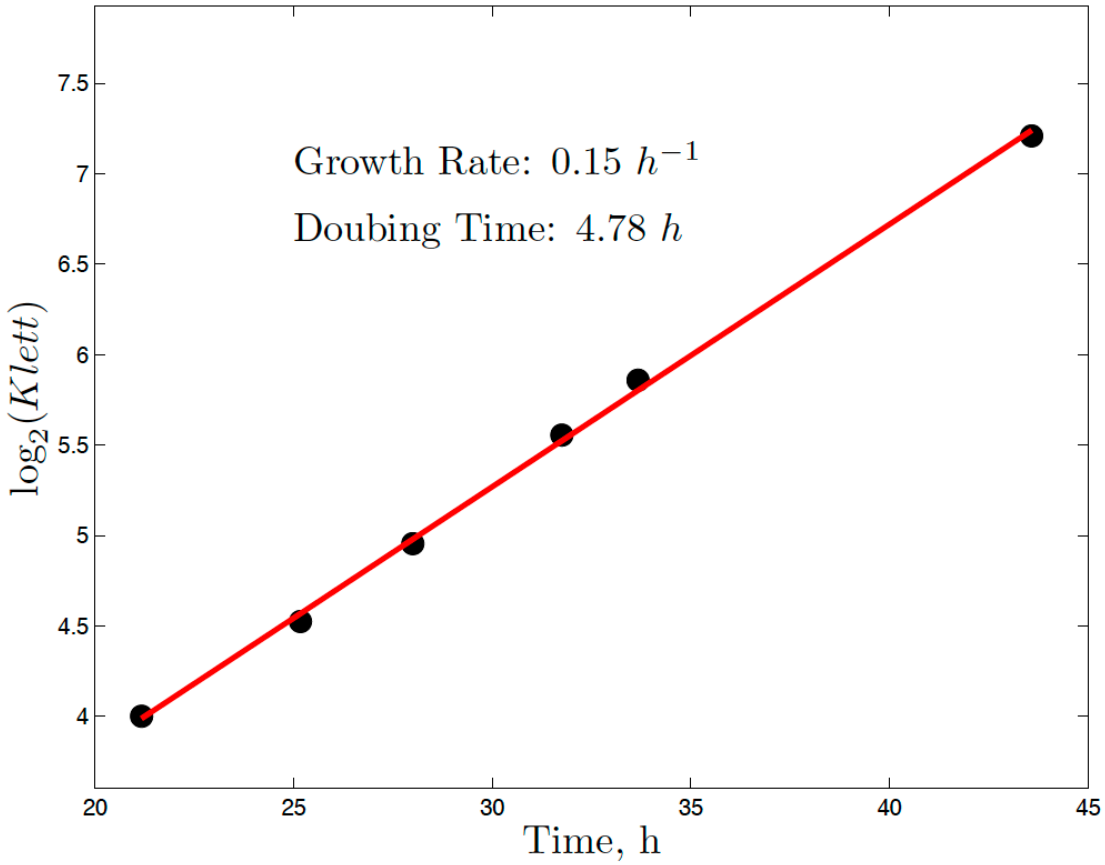

Figure 2. *DBY11369* was grown in $100mM$ ethanol media as a batch culture

For the chemostat experiments, we chose a concentration of $30mM$ ethanol since it gave optimal biomass and was well within the linear range. The fact that $30mM$ ethanol is limiting for growth in batch implies that it is likely to be liming for steady–state growth in chemostats but does not guarantee that. Therefore, we experimentally tested whether $30nm$ ethanol is indeed limiting at steady–state. We grew *DBY11369* at $\mu = 0.10h^{-1}$ to steady–state feeding from media containing $30mM$ ethanol and using a Coulter counter measured a cell density of 1.5×10^7 *cells/mL*. Then we switched to media with identical composition except for two times higher ethanol concentration ($60mM$). When the culture reached steady–state (again at $\mu = 0.10h^{-1}$), we measured culture density of 3×10^7 *cells/mL* indicating that $30mM$ ethanol is indeed limiting and in the linear response regime not only for batch but also for continuous steady–state cultures of *DBY11369*.

We used the same type of experiments to establish optimal limiting concentrations for PO_4^{3-} and NH_4^+, Fig.S4. The optimal concentrations chosen for the chemostat experiments and verified to be limiting at steady–state are $[KH_2PO_4] = 20mg/L$ and $[(NH_4)_2SO_4] = 100mg/L$.

The determined amounts for the limiting nutrients were mixed with minimal defined (MD) media, metals, and vitamins. The only carbon source in all cases was ethanol $30mM$ for the ethanol limitation and ($100mM$) for the nitrogen and phosphorus limitations. All media was added via sterile filtration to autoclaved carboys as described

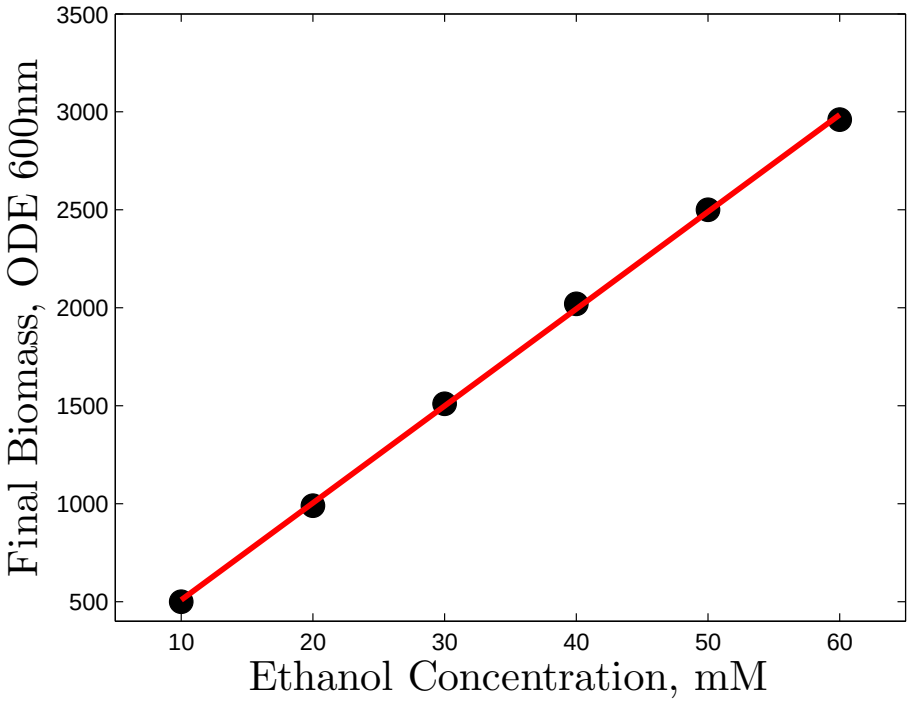

Figure 3. Dependence of the final biomass of *DBY11369* grown as a batch culture in chemostat media on the initial concentration of ethanol.

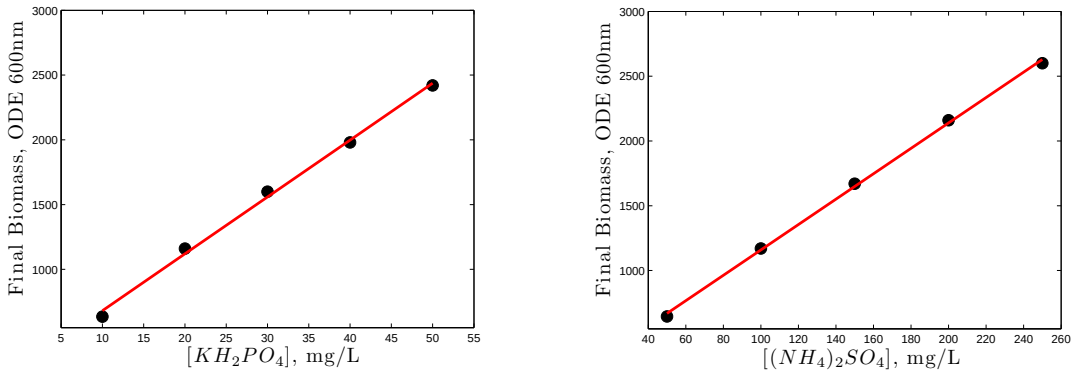

Figure 4. Dependence of the final biomass of *DBY11369* grown as a batch culture in chemostat media on the initial concentration of phosphate (PO_4^{3-}) and on the initial concentration of ammonium, (NH_4^+)

previously (Brauer et al., 2005, 2008; Saldanha et al., 2004).

3 Distributions of Cell Size

The cell–size distributions in all limitations (Fig.S5) show very good reproducibility as demonstrated by the close overlap of the red traces corresponding to individual measurements. Since in all cases the samples analyzed

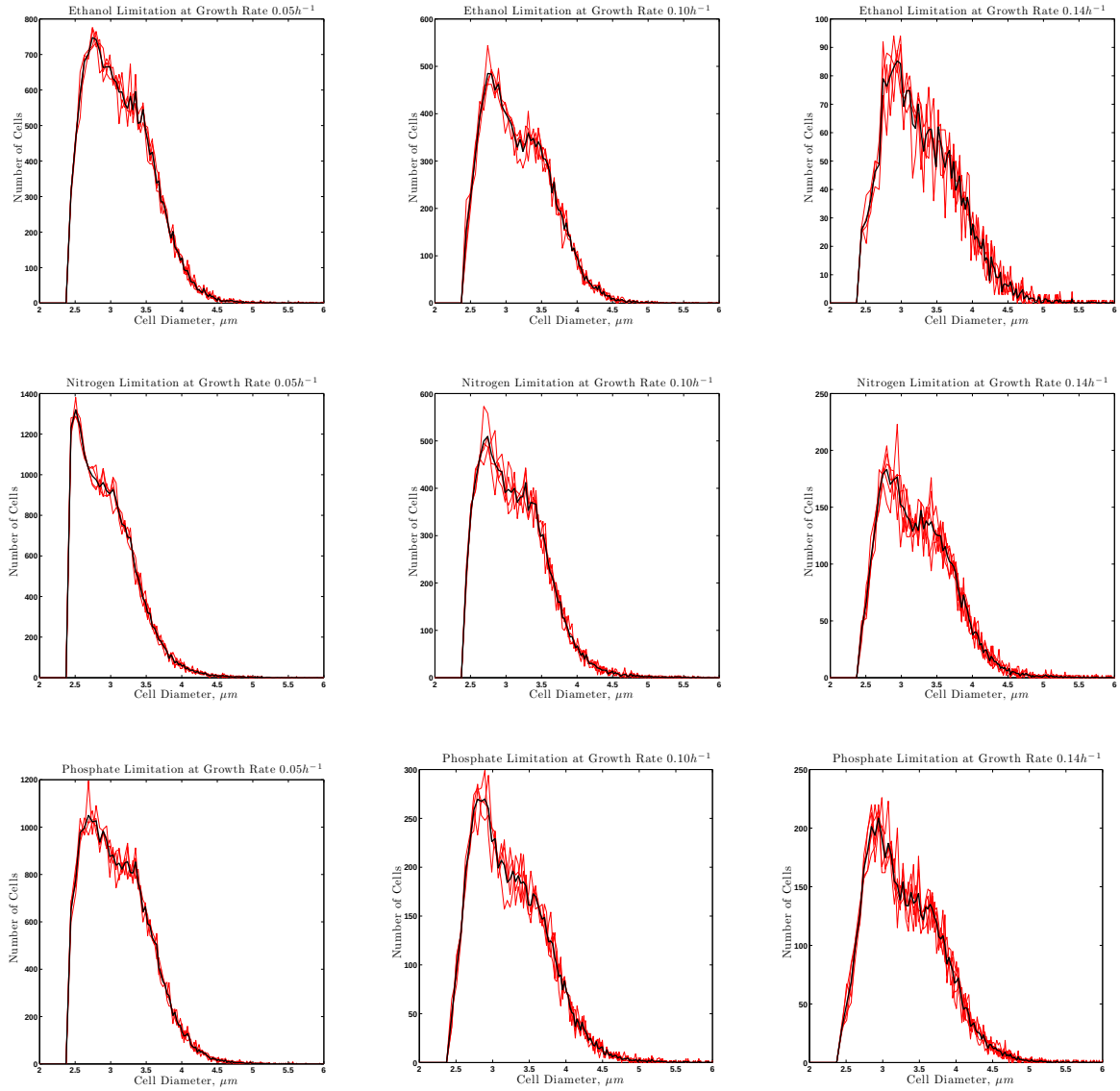

Figure 5. Distributions of cell sizes as a function of the growth rate across nutrient limitations of cultures using ethanol carbon source. The red traces are individual measurements and the black curves are the average of the individual measurements.

on the Coulter counter where diluted $1/1000$, the highest growth rates having the lowest biomass (Fig.1 from the paper) exhibit higher noise levels. The cell–size distributions in all limitations Fig.S5 show a growth rate

trend of increased variance with the growth rate due to increasing fraction of cells with larger diameters, Fig.S5. Furthermore, some distributions, such as the cell–sizes of the ethanol limitation at $\mu = 0.10h^{-1}$ appear to be bimodal. The most likely reason for this trend is the increased fraction of budded cells as indicated by Fig.1 from the paper. Based on this argument, we developed and fit a model explaining the observed cell–size distributions as a mixture of the two populations (budded and non–budded cells) with different cell–size distributions, Fig.S6. First, we fit a mixture of Gaussian distributions to all data but the model gave rather large systematic deviations

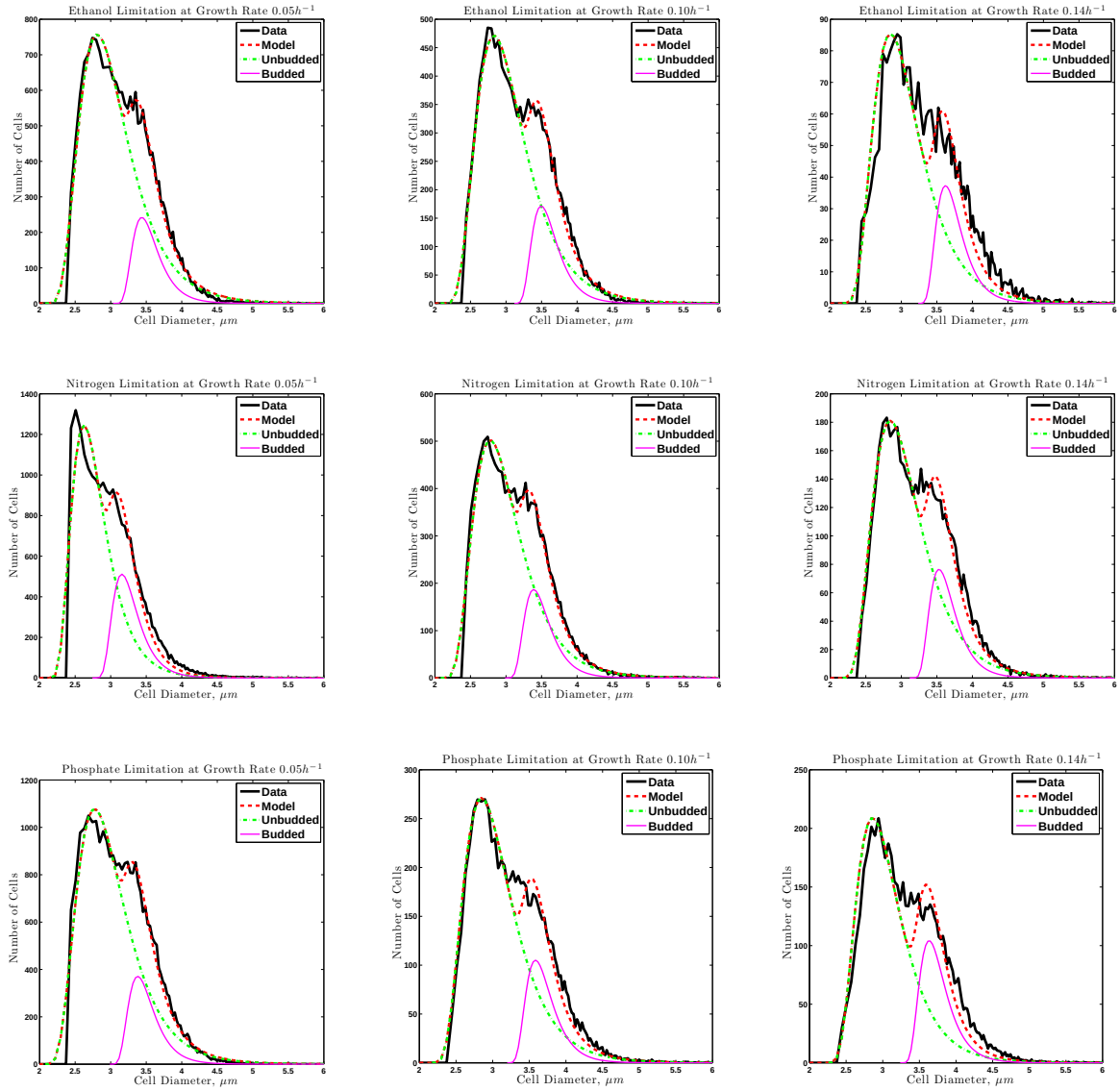

Figure 6. The empirical distributions (black) of cell sizes are decomposed into a mixture of two distributions, non-budded cells (green) and budded cells (magenta). The cell–size distribution predicated by the model (a superposition of the budded and non-budded distributions) is plotted as dotted red curves.

from the data. The reason for those deviations is the significant asymmetry in the measured distributions, Fig.S5. Thus generalized Gaussian distributions were used resulting in a much better fit to the data without significant systematic deviations, Fig.S6. Why can be a reason for the cell–size distributions to follow generalized rather than simple Gaussian distributions? A very simple and likely explanation is the non–linearity in the interactions of the factors that determine cell size in yeast. A Gaussian distribution is expected based on the Central Limit Theorem which is derived and proved based on the assumption of linear superposition of many independent factors. If the cumulative effect of the factors determining cell–size is not based on simple summation of their individual effects and/or those factors are not independent (both of which are very likely) the expected distribution is more likely to be generalized Gaussian as the data indicate, Fig.S5.

The model fits depicted on Fig.S6 can be used to infer the fraction of budded cells. To evaluate the accuracy of this inference, we compare the model predication to the experimentally measured budded fraction, Fig.S7. While

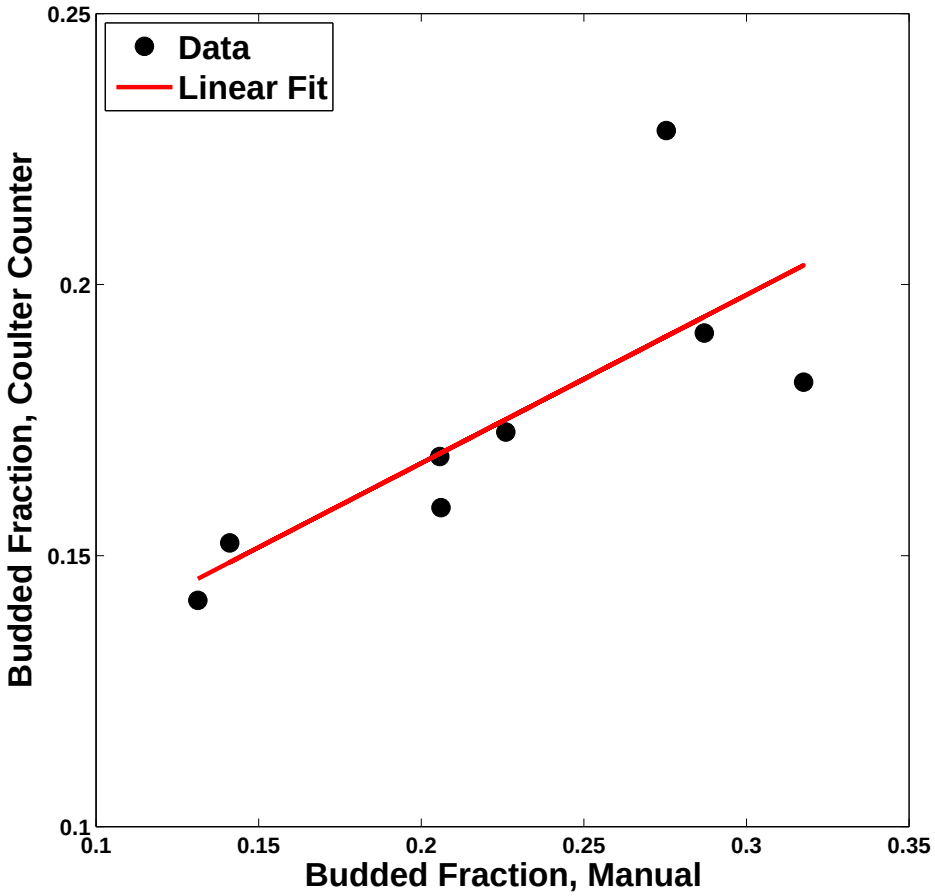

Figure 7. Bud Index Comparison. The fraction of budded cells predicted by the model of distribution sizes is plotted versus the fraction of budded cells counted experimentally, see Fig.1 from the paper

the model prediction and the measurement show strong correlation, the deviation at the highest growth rates are significant which is most likely due to the noisier data because of the lowest biomass density at the highest growth rates Fig.1 from the paper. More significantly, the intercept of the linear fit does not go through $(0, 0)$ which most likely is caused by different shapes of the distributions of budded and non–budded cells. Indeed, adding a fudge parameter for different shapes moves the intercept toward zero and further improves the fit to the data.

4 Modeling the Transcriptional Growth Rate Response

A useful way to analyze the growth rate data is to fit a model that captures the growth rate response trends. Given the limited number of datapoints per gene, only simple models can be used without over–fitting the data. The explicit form of the model that should describe the data is hard to derive based on first principles. Among the simplest models is a linear model with two parameters per gene, one parameter for the mean nutrient specific level and one in which the mRNA concentration depends linearly on the growth rate, $mRNA_i = a_i\mu + b_i$. Based on sigmoidal Hill function (or as a sub case Michaelis Menten) signal transduction transfer functions and using some approximations, one may expect a power–law dependence (also needing 2 parameters per gene) between the growth rate (μ) and the change in mRNA levels, $mRNA_i = b_i\mu^{a_i}$. Brauer et al. (2008) and Airoldi et al. (2009) used a model with 2 parameters per gene with exponential dependence between the mRNA level and the growth rate, $mRNA_i = b_i e^{a_i\mu}$. In semi–log space, such exponential model "appears" linear $\log(mRNA_i) = \log(b_i) + a_i\mu$. Similarly, in log–log space the power–law model becomes linear, $\log(mRNA_i) = \log(b_i) + \log(\mu)a_i$.

An unbiased way to assess the performance of those models (having the same level of complexity) is to use the fraction of variance in the data explained by the model over the total variance in the data as quantified by R^2, equation 5. The distributions of R^2 for a power–law and an exponential (linear in semilog space) models are shown in Fig.S8. Based on goodness of fit as quantified by R^2, the power–law model captures the largest fraction of the

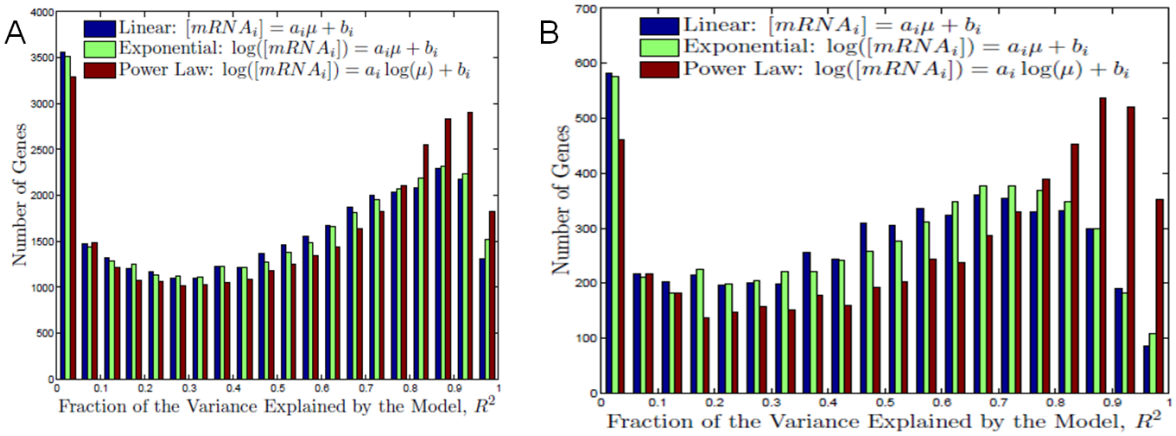

Figure 8. Explained fraction of the variance in the gene expression data on glucose carbon source by a linear, power–law and an exponential models. The data for all 6 growth rates $\mu = \{0.05, 0.10, 0.15, 0.20, 0.25, 0.30\}h^{-1}$ from the (Brauer et al., 2008) experiments was used by all. A) All nutrient limitations and B) Uracil limitation.

variance for all limitations (Fig.S8A) and especially on some limitations, such as uracil Fig.S8B. Since Brauer

et al. (2008) used the exponential model and our use of a model is phenomenological (to quantify trends in the transcriptional growth rate response), throughout our paper we use *only* the exponential model for consistency. In semi–log space, the exponents in the model "appear" to be slopes, and thus we will use the term slopes in keeping with previous work (Brauer et al., 2008).

$$R_j^2 = 1 - \frac{\sum_{i\in\alpha}(y_{ij} - f_{ij})^2}{\sum_{i\in\alpha}(y_{ij} - \bar{\mathbf{y}}_j)^2} \tag{5}$$

In (5), $\mathbf{y}_j$ is a vector of expression levels of the j^{th} gene (j^{th} column in $\mathbf{Y}$), $\bar{\mathbf{y}}_j$ is its mean expression level, i is index enumerating the set of conditions α used in the model and f_{ij} is the model predication for the i^{th} condition and j^{th} gene.

4.1 Universal Growth Rate Response

To understand some aspects of the growth rate response, one has to look at growth rate response specific to nutrient limitations and to subgroups of limitations. Such specific growth rate responses are discussed in the following section. Here, we first consider the growth rate response that is common to all limitations on both glucose and ethanol carbon source. To identify such universal growth rate response, we fit a regression model explaining the expression levels of each gene with a single gene specific slope. For comparison to previous work (Brauer et al., 2008), we also fit models that incorporate nutrient specific constants reflecting the mean expression of each gene for each nutrient. The goodness of fit is quantified by R^2, (5). Then, the data for each gene is permuted 10^6 times and the R^2 for each permutation is computed. Based on these computations, the significance of the growth rate response for each gene is quantified by a *p value* which equals the fraction of R^2 values in the permuted data that are larger than the R^2 for the non–permuted data, Fig.S9. It might be tempting to interpret the high R^2 and low *p–*

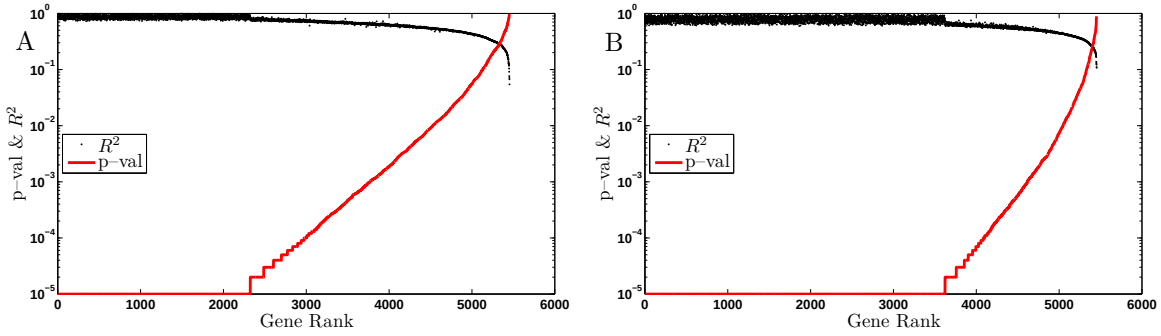

Figure 9. Rank ordered p values and the corresponding R^2 from a model accounting for both the nutrient mean effect (by a nutrient specific constant) and for the growth rate response by a gene specific slope, (Brauer et al., 2008). (A) Results for carbon, nitrogen and phosphate limitations on glucose and ethanol carbon source and (B) Results for all limitations on glucose and ethanol carbon source.

vals (Fig.S9) as evidence for universal growth rate response shared by half the genome, Fig.S9A or even $3/4$ of the genome, Fig.S9B. Yet this conclusion overlooks the fact that the model includes *both* the growth rate *and* the effect of the nutrient limitation on the mean level of gene expression. Therefore, a gene whose mean expression level

differs significantly among limitations and carbon sources will fit the model well (high R^2) even if its slopes on individual limitations differ significantly; As long as most of the variance in the expression of such a gene comes from different limitation–specific mean levels, its R^2 will always be high independent of its slope on different limitations. The significance of the fit for such a gene is further bolstered by the large amount of high quality data coming from many limitations, Fig.S9B. Prime examples for genes in this group are genes involved in ethanol utilization and gluconeogensis. In particular, genes such as the cytoplasmic malate dehydrogenase *MDH2* that have large positive slopes in all ethanol carbon source limitations and large negative slopes in all glucose carbon source limitations fit the models with relatively large negative slope and high R^2. The reason for the high R^2 is that most of the variance in the data for *MDH2* comes from the much higher level of expression of *MDH2* on ethanol carbon source and the model explains this variance well because of the nutrient specific constant. The net negative slope reflects the fact that there are more glucose carbon source conditions and a net negative slope minimizes the sum of squared residues. At a more conceptual level, the fact that adding more limitations in Fig.S9B compared to Fig.S9A increases the number of genes with very significant fits indicates that a model taking in account both the nutrient mean level and the growth rate slope is not optimal for identifying a common growth rate response. The number of genes with a common growth rate response can only decrease (but not increase) by adding more conditions. The increase in the number of genes for which the model explains a significant fraction of the variance reflects the fact that the larger the set of profiled conditions, the more likely that a gene will be expressed differentially for at least one of the conditions.

4.2 Predicting Growth Rate from Gene Expression

Many of the genes with universal growth rate response and very high R^2 used for predicting growth rate are strongly correlated to each other and thus represent redundant information. As a result a subset of those genes may predict growth rate just as accurately. To choose such subset we used $\ell 1$-regularized regression, (Malioutov et al., 2005).

5 Biological Functions with Significant Growth Rate Responses

The clustergram of GO terms in the paper provides a high–level comprehensive overview of the growth rate response of genes from various functional groups. To go beyond the high–level summary, we explore in more details the distributions of growth rate responses of the sets of genes defined based on the Gene Ontology and different expression levels in auxotrophic and prototrophic cultures. We start with functional groups whose growth rate response is expected and then more toward more unexpected results.

5.1 *Gene set 1:* Mitochondrial envelope

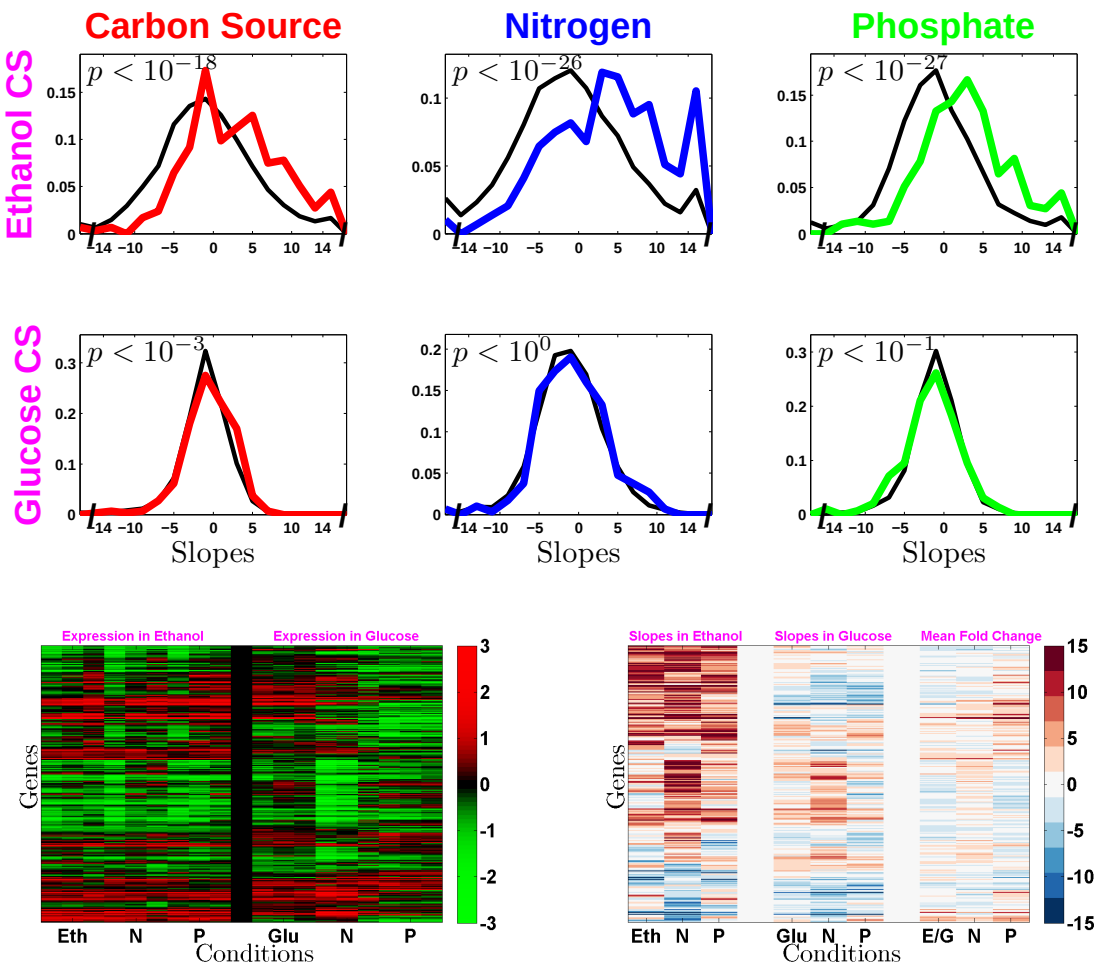

Figure 10. Mitochondrial envelope. Interactive Plots The top panel of distributions corresponds to ethanol carbon source and the bottom one to glucose carbon source. Each column corresponds to a limitation (carbon source, nitrogen and phosphate) as indicated on the top. The black distributions in each panel are for all genes in the genome and the colored distributions are for mitochondrial envelope genes only. The clustergrams display gene expression (left) and slopes & fold changes (right). The corresponding rows in the two clustergrams display data for the same genes and the clustering (permutation) is based on similarity metric (non–centered correlations) computed using *only* the slopes data (left panel).

Consistent with the requirement for increased aerobic–respiration at fast growth on ethanol carbon source, many mitochondrial genes have positive slopes. This trend is illustrated with the mitochondrial envelope genes, Fig.S10. The genes with positive slopes are the same across all limitations on ethanol carbon source, first set of three columns in the clustergram of slopes. Interestingly a subset of the genes with positive slopes in ethanol also have positive slopes in glucose carbon source. Once again the nitrogen limitations (middle columns in the first and

second sets of columns of the slopes clustergram) are similar to each other and stand apart from the carbon and phosphate limitations.

5.2 *Gene set 2:* Cellular respiration

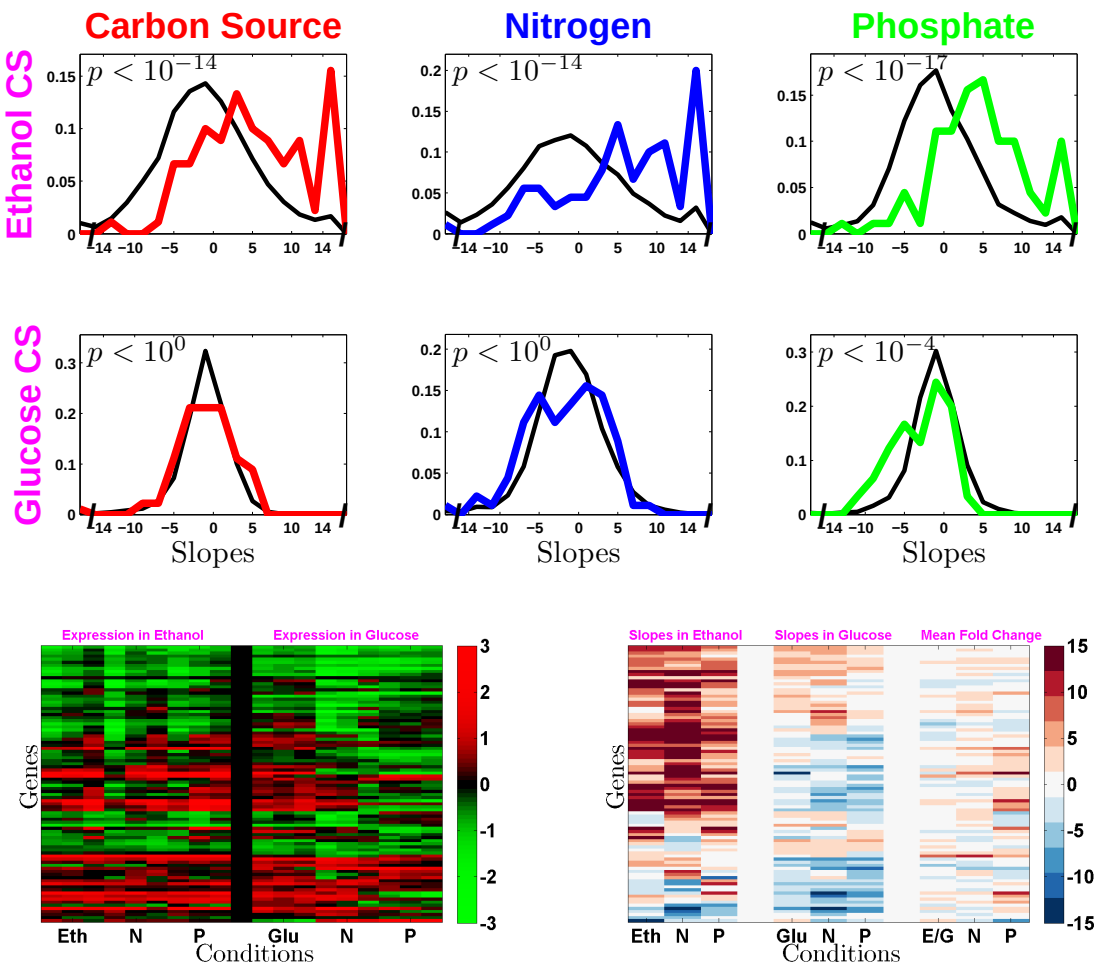

Figure 11. Cellular respiration Interactive Plots Notation is the same as in Fig.S10 with colored distributions corresponding to the slopes of genes involved in cellular respiration.

Similar to gene set 1, growth rate related increase in the expression of cellular respiration genes is expected for cultures growing on ethanol carbon source.

5.3 *Gene set 3:* Generation of precursor metabolites and energy

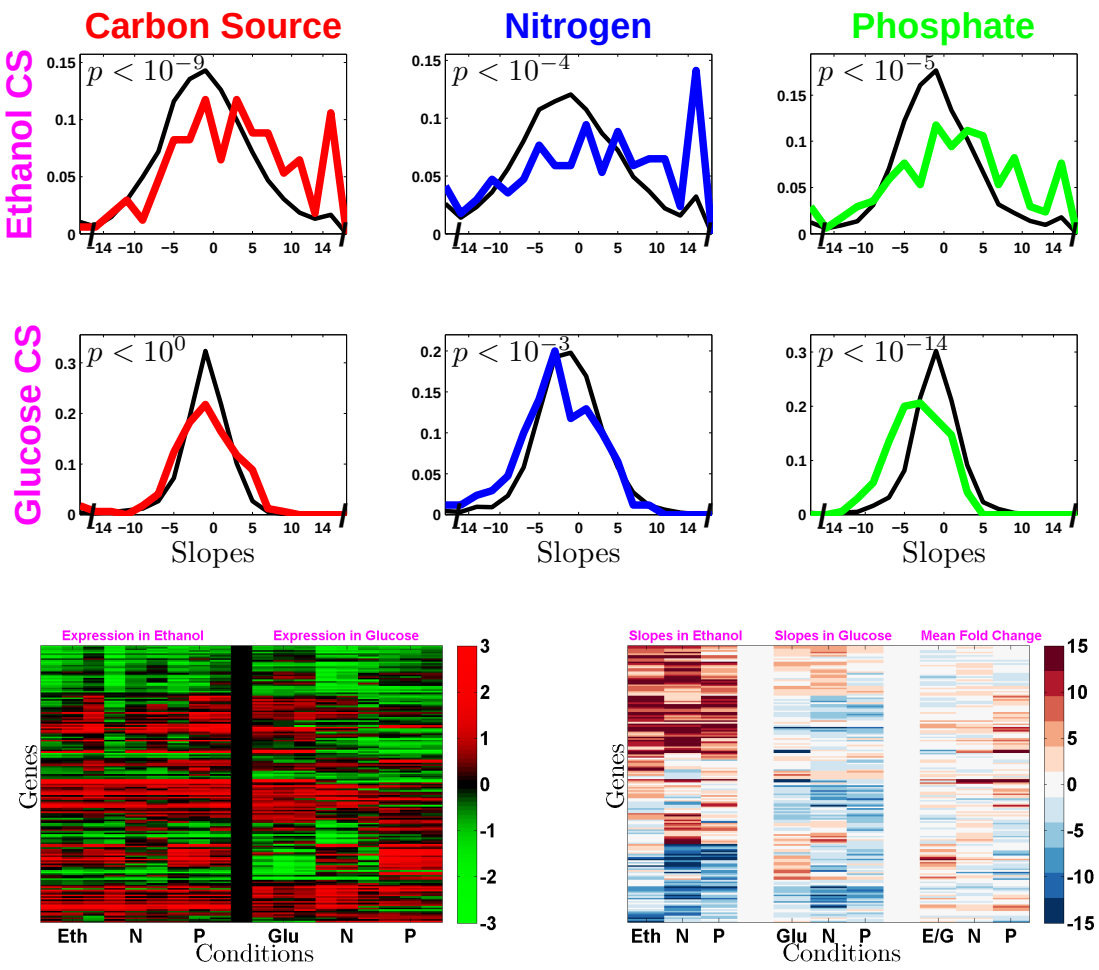

Figure 12. Generation of precursor metabolites and energy. See Interactive Plots. Notation is the same as in Fig.S10 with colored distributions corresponding to the slopes of genes involved in generation of precursor metabolites and energy.

Some of the genes in this set are mitochondrial such as the TCA cycle (Fig.10 from the paper) which explains at least in part the significantly positive slopes of this set of genes. In fact given the central role of precursor metabolites and energy in growth the more surprising funding is that this set of genes does not have significantly positive slopes on glucose carbon source.

5.4 *Gene set 4:* Vacuole

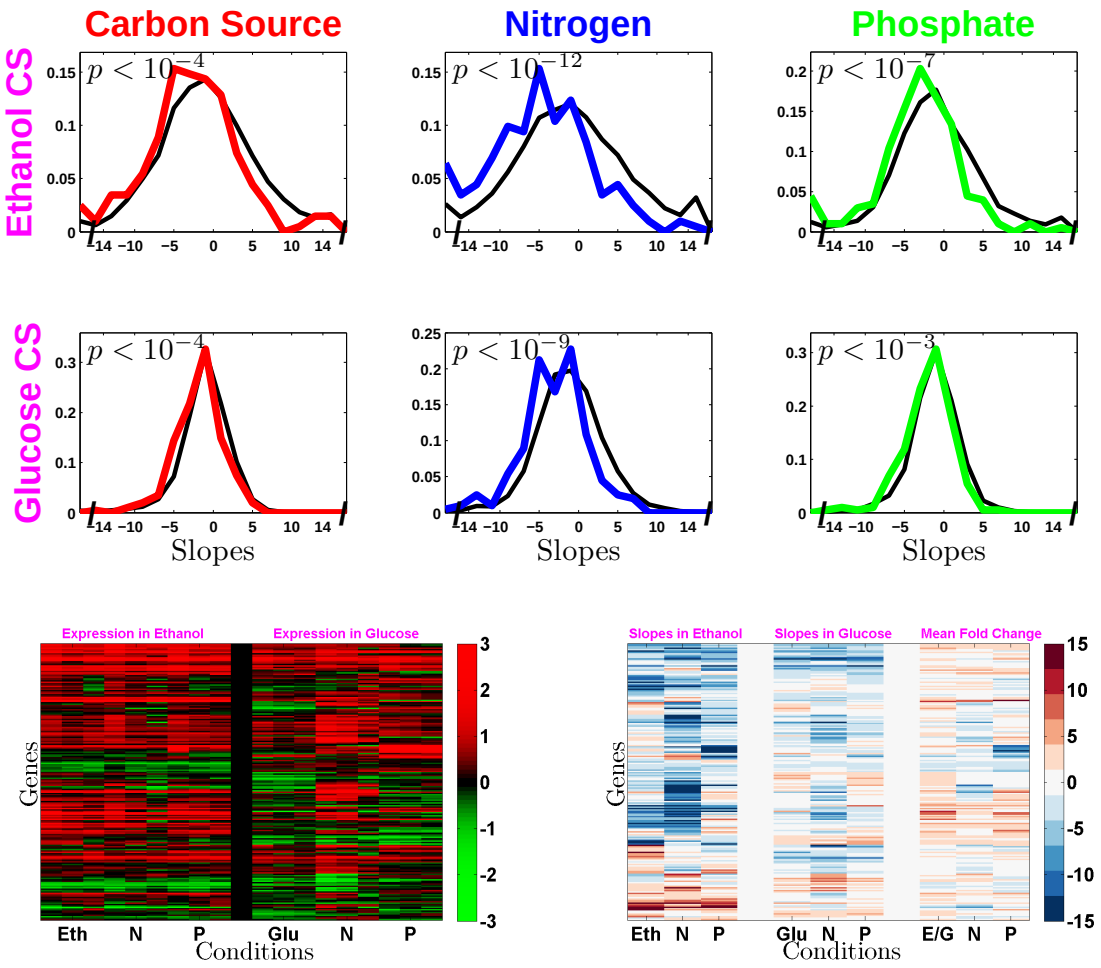

Figure 13. Vacuole. See Interactive Plots. Notation is the same as in Fig.S10 with colored distributions corresponding to the slopes of vacuolar genes.

The vacuoles are part of the universal growth rate response, which most likely reflects the increased rate of recycling in slowly growing cells. The distribution of slopes for the vacuole genes is shifted significantly toward negative slopes (left) across all limitations on all carbon sources. This effect is particularly strong in the nitrogen limited cultures, middle column of distributions, Fig.S13. Again the genes with negative slopes are the same across limitations (as evident from the clustergram of slopes), especially the ones on ethanol carbon source.

5.5 *Gene set 5:* Peroxisome

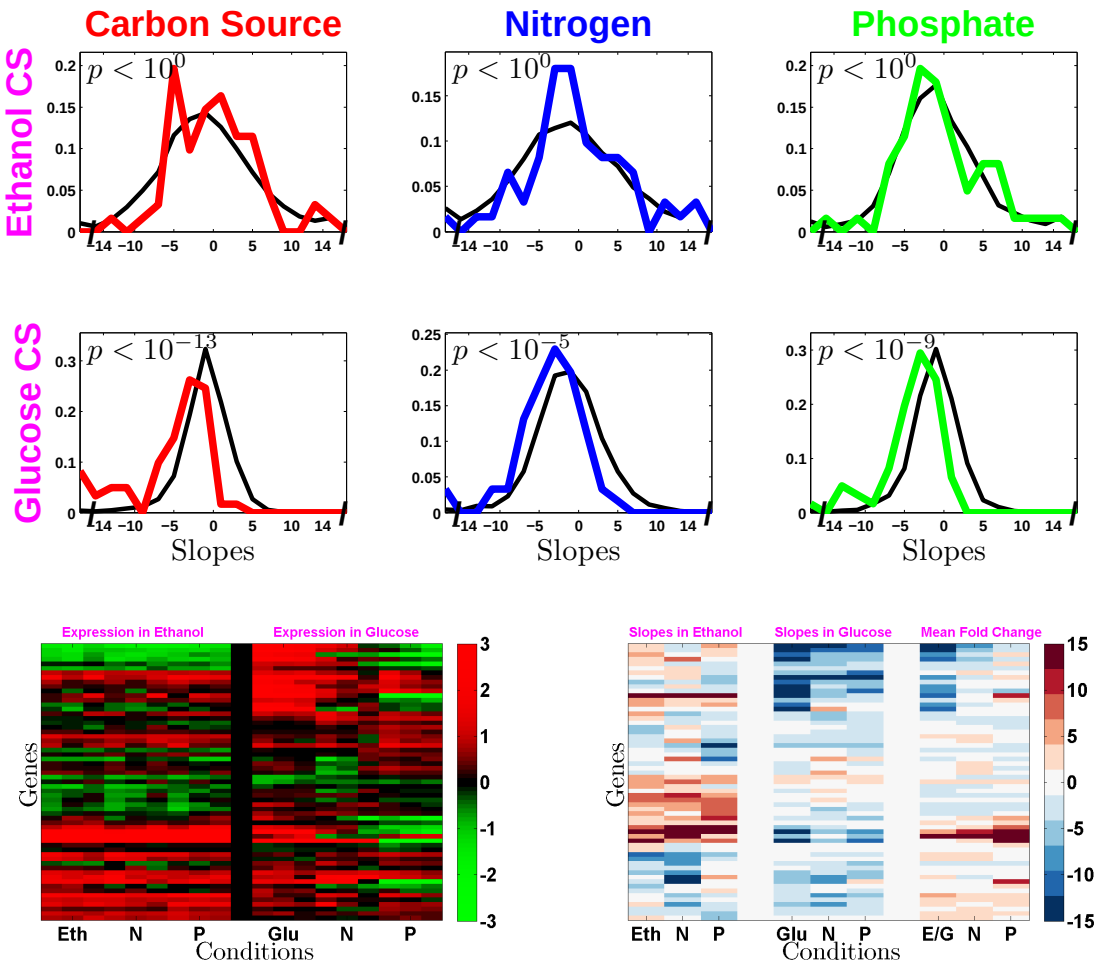

Figure 14. Peroxisome. Interactive Plots. Notation is the same as in Fig.S10 with colored distributions corresponding to the slopes of peroxisomal genes.

As noted by Brauer et al. (2008), peroxisomal genes are overrepresented among the genes with negative slopes as revealed here by the distribution of slopes for peroxisomal genes being shifted significantly to the left for all limitations on glucose carbon source. Interestingly, this is not the case for ethanol carbon source, top row of distributions, Fig.S14.

5.6 *Gene set 6:* Cofactor metabolic process

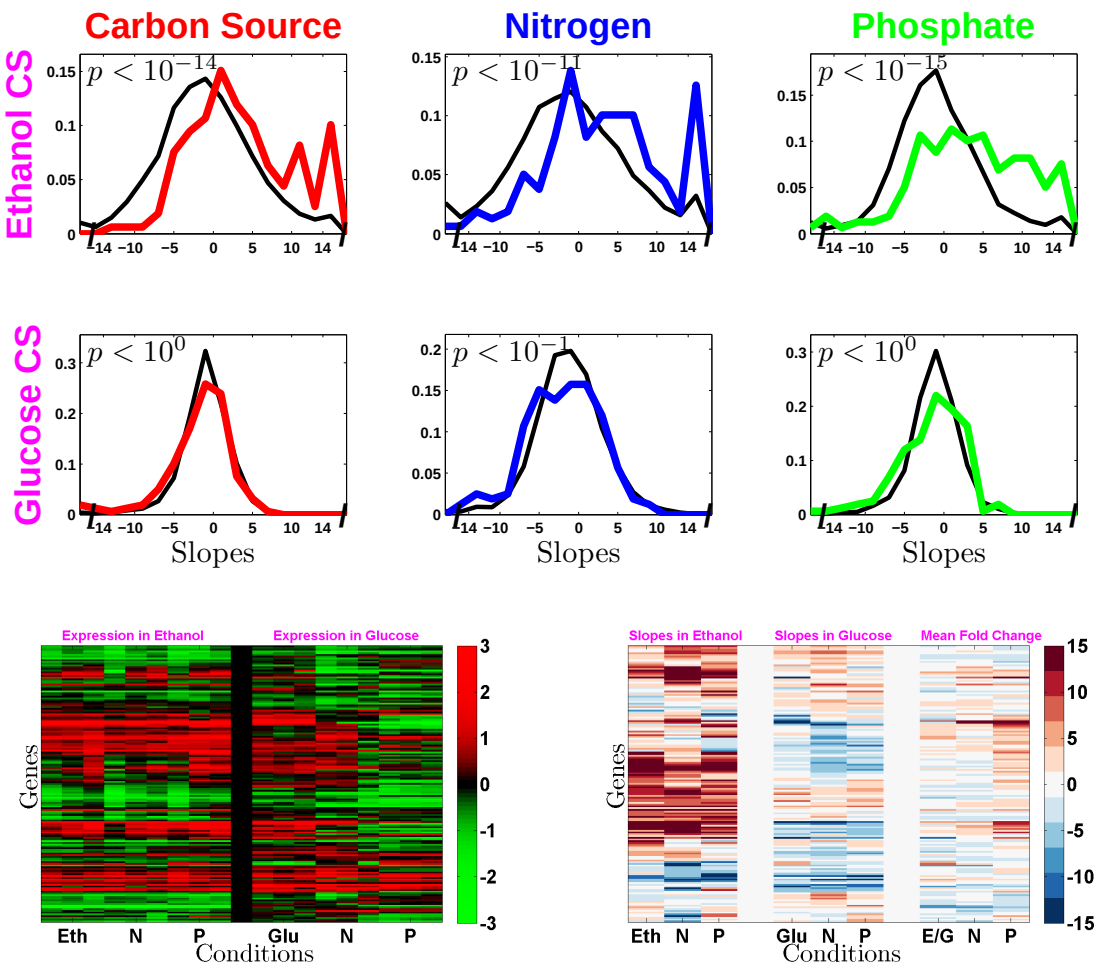

Figure 15. Cofactor metabolic process. Interactive Plots. Notation is the same as in Fig.S10 with colored distributions corresponding to the slopes of genes involved in cofactor metabolic processes.

A diverse group of genes involved in the synthesis of cofactors or using cofactors have significantly positive slopes in ethanol carbon source across all limitations. A subset of those genes also have modestly positive slopes in glucose across all limitations but as a whole for glucose carbon source the slopes of this gene set is not significantly different from the slopes for all genes.

5.7 *Gene set 7:* Microtubule organizing center

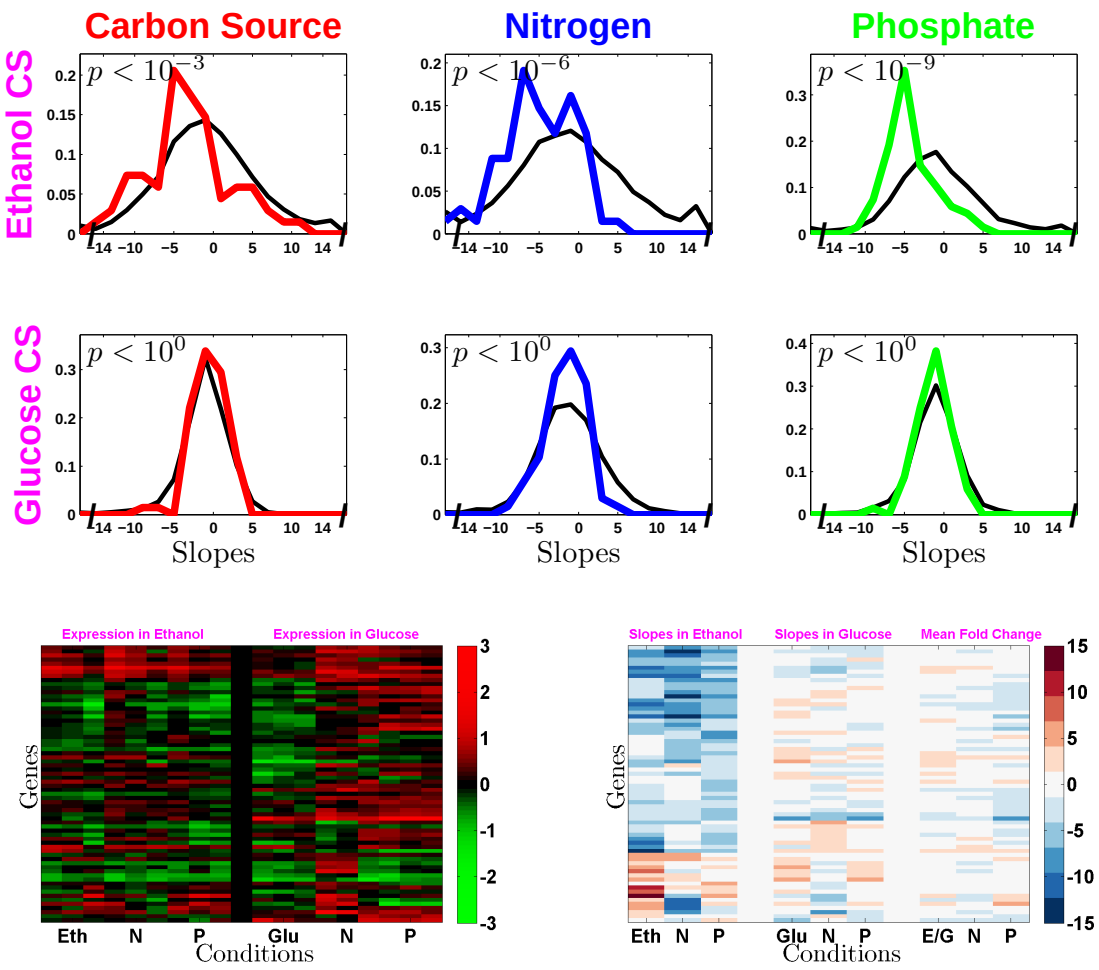

Figure 16. Microtubule organizing center. See Interactive Plots. Notation is the same as in Fig.S10 with colored distributions corresponding to the slopes of genes involved in the microtubule organizing center.

Some cell division cycle (CDC) related genes, including DNA replication, chromosome segregation, and microtubule organizing center have significantly negative slopes as exemplified here, Fig.S16. The clustergram of slopes (Fig.S16) indicates that the genes with negative slopes are the same across all limitations on ethanol carbon source.

5.8 *Gene set 8:* Heterocycle metabolic process

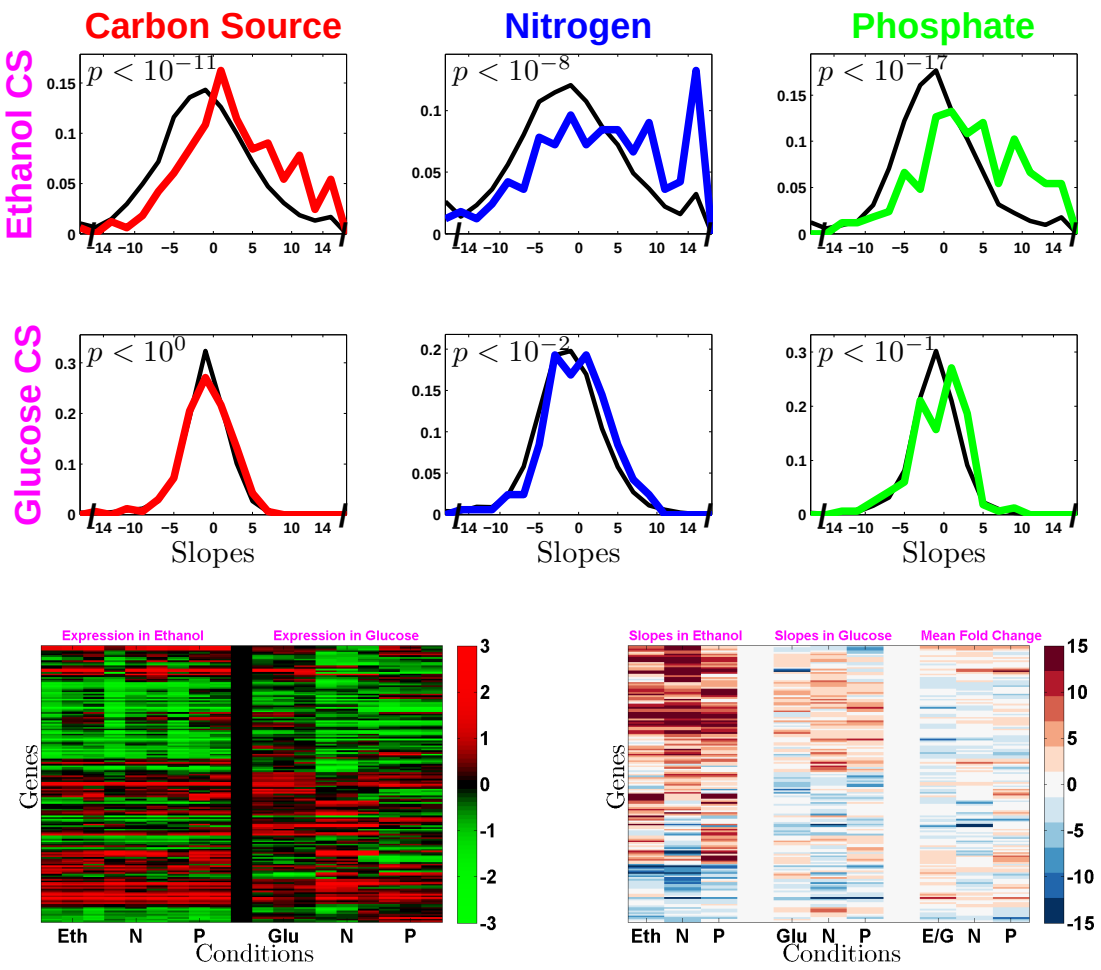

Figure 17. Heterocycle metabolic process. Interactive Plots. Notation is the same as in Fig.S10 with colored distributions corresponding to the slopes of genes involved in heterocycle metabolic process.

This set includes genes participating in the biosynthesis of histidine, purines, pyrimidines, thiamine, and other heterocyclic compounds. Since all these compounds are required for biomass production and growth its not surprising to see the growth rate induction of the genes involved in their biosynthesis. Interestingly, these genes are induced to a smaller extent in cultures growing on glucose carbon source.

5.9 *Gene set 9:* Vitamin metabolic process

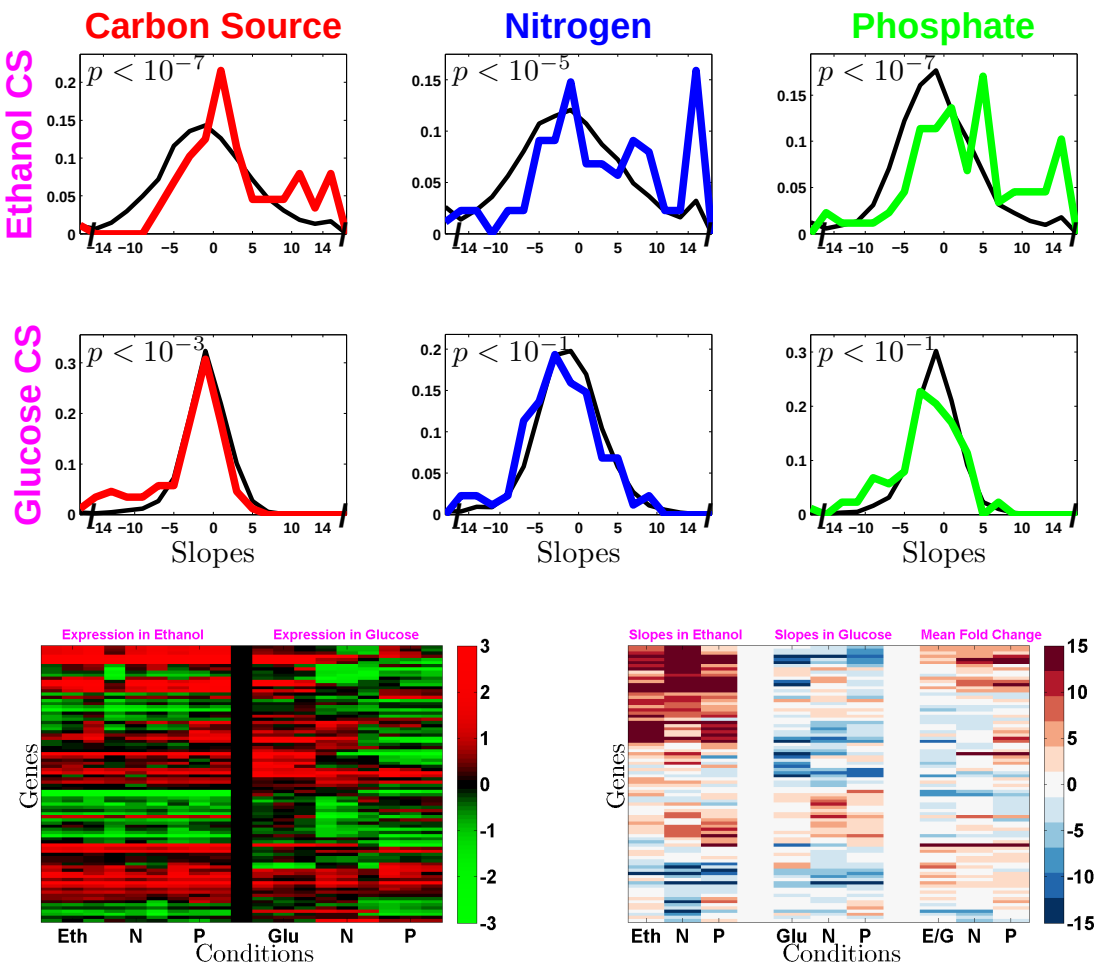

Figure 18. Vitamin metabolic process Interactive Plots Notation is the same as in Fig.S10 with colored distributions corresponding to the slopes of genes involved in heterocycle metabolic process.

Many of the vitamin related genes in this group are cofactors for mitochondrial enzymes that show transcriptional induction themselves, such as the enzymes catalyzing the TCA cycle, see Fig.10 from the paper. Thus up–regulation of gene from this set is another indicator of growth rate induced increase in the TCA cycle flux and related biochemical reactions involved in the production of energy and intermediate metabolites.

5.10 *Gene set 10:* Cell Division Cycle

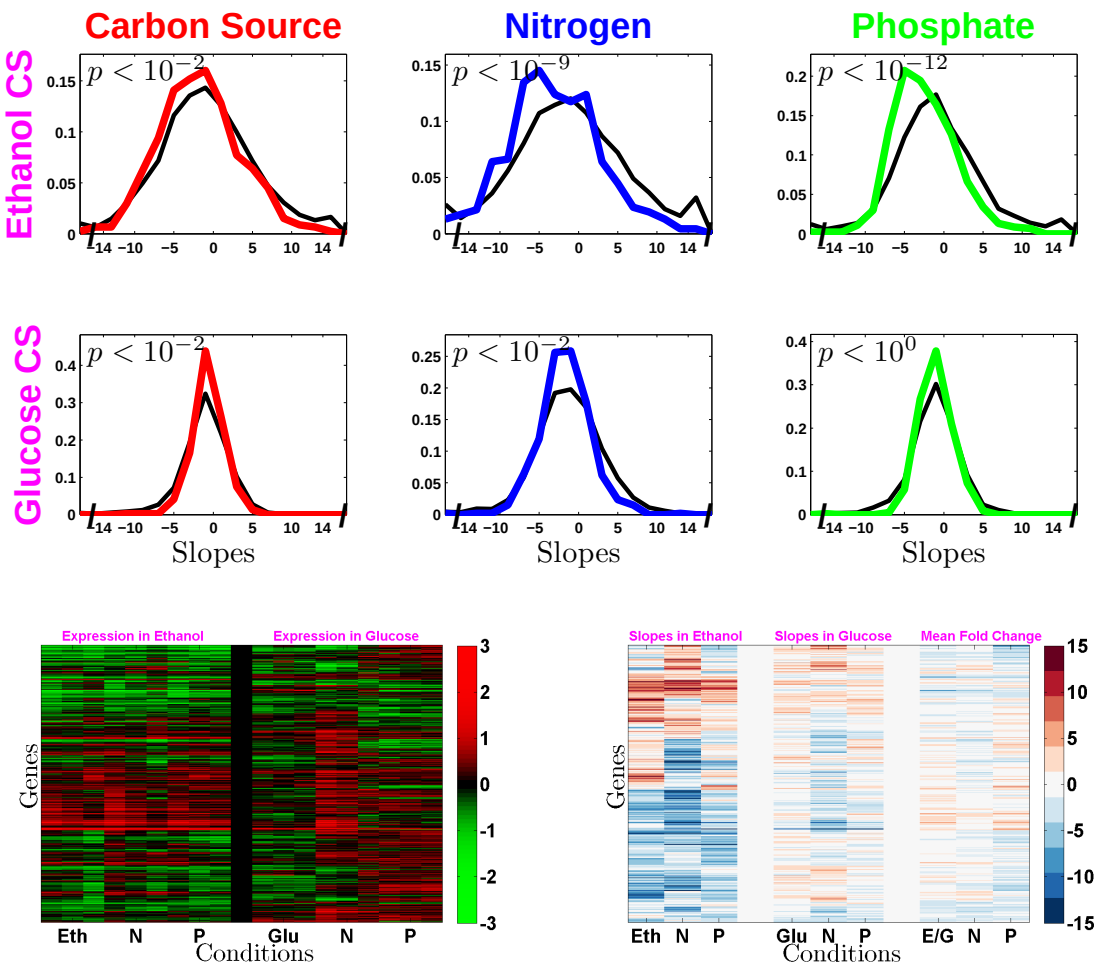

Figure 19. Cell Division Cycle Interactive Plots Notation is the same as in Fig.S10 with colored distributions corresponding to the slopes of genes involved in the cell division cycle.

5.11 *Gene set 11:* Oxidoreductase activity

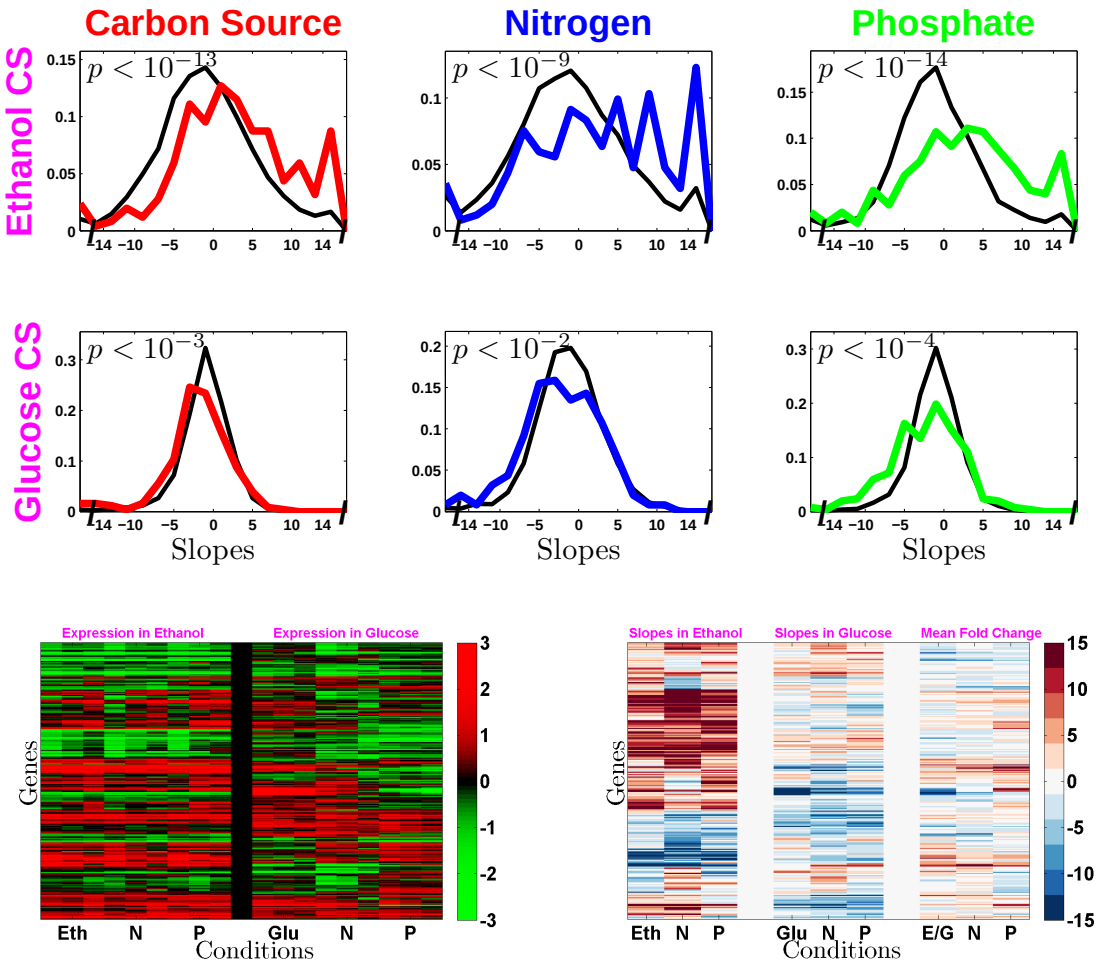

Figure 20. Oxidoreductase activity Interactive Plots Notation is the same as in Fig.S10 with colored distributions corresponding to the slopes of genes involved in oxidoreductase activity.

References

Edoardo M. Airoldi, Curtis Huttenhower, David Gresham, Charles Lu, Amy A. Caudy, Maitreya J. Dunham, James R. Broach, David Botstein, and Olga G. Troyanskaya. Predicting cellular growth from gene expression signatures. *PLoS Comput Biol*, 5(1):e1000257, 2009. doi: 10.1371/journal.pcbi.1000257. URL http://dx.doi.org/10.1371/journal.pcbi.1000257.

Matthew J. Brauer, Alok J. Saldanha, Kara Dolinski, and David Botstein. Homeostatic adjustment and metabolic

remodeling in glucose-limited yeast cultures. *Molecular Biology of the Cell*, 16(5):2503–2517, May 2005. ISSN 1059-1524. doi: 10.1091/mbc.E04-11-0968. PMID: 15758028 PMCID: 1087253.

Matthew J. Brauer, Curtis Huttenhower, Edoardo M. Airoldi, Rachel Rosenstein, John C. Matese, David Gresham, Viktor M. Boer, Olga G. Troyanskaya, and David Botstein. Coordination of growth rate, cell cycle, stress response, and metabolic activity in yeast. *Mol. Biol. Cell*, 19(1):352–367, 2008. doi: 10.1091/mbc.E07-08-0779. URL http://www.molbiolcell.org/cgi/content/abstract/19/1/352.

Dmitry Malioutov, Mjdat etin, and Alan S. Willsky. Homotopy continuation for sparse signal representation. In *In Prceedings of the IEEE International Conference on Acoustics, Speech, and Signal Processing*, pages 733–736. IEEE Press, 2005.

Jacques Monod. Recherches sur la croissance des cultures bacteriennes. *Paris:Herman*, 1942.

Jacques Monod. The growth of bacterial cultures. *Annual Review of Microbiology*, 3:371–394, 1949.

A. Novick and L. Szilard. Description of the chemostat. *Science*, 112(2920):715–716, 1950. ISSN 0036-8075. doi: 10.1126/science.112.2920.715. URL http://www.sciencemag.org/cgi/content/citation/112/2920/715.

Alok J. Saldanha, Matthew J. Brauer, and David Botstein. Nutritional homeostasis in batch and Steady-State culture of yeast. *Mol. Biol. Cell*, 15(9):4089–4104, September 2004. doi: 10.1091/mbc.E04-04-0306. URL http://www.molbiolcell.org/cgi/content/abstract/15/9/4089.